

(12) INTERNATIONAL APPLICATION PUBLISHED UNDER THE PATENT COOPERATION TREATY (PCT)

(19) World Intellectual Property
Organization
International Bureau



(10) International Publication Number
WO 2020/148644 A1

(43) International Publication Date
23 July 2020 (23.07.2020)

(51) International Patent Classification:

C01B 32/198 (2017.01) *A01G 15/00* (2006.01)
C01B 33/00 (2006.01) *B82Y 30/00* (2011.01)

Declarations under Rule 4.17:

— *of inventorship (Rule 4.17(iv))*

(21) International Application Number:

PCT/IB2020/050259

Published:

— *with international search report (Art. 21(3))*
— *in black and white; the international application as filed contained color or greyscale and is available for download from PATENTSCOPE*

(22) International Filing Date:

14 January 2020 (14.01.2020)

(25) Filing Language:

English

(26) Publication Language:

English

(30) Priority Data:

62/791,927 14 January 2019 (14.01.2019) US

(71) Applicant: **KHALIFA UNIVERSITY OF SCIENCE AND TECHNOLOGY** [AE/AE]; P.O. Box 127788, Abu Dhabi 127788 (AE).

(72) Inventors: **ZOU, Linda**; c/o Khalifa University of Science and Technology, P.O. Box 127788, Abu Dhabi 127788 (AE). **LIANG, Haoran**; c/o Khalifa University of Science and Technology, P.O. Box 127788, Abu Dhabi 127788 (AE).

(74) Agent: **AL TAMIMI AND COMPANY**; Precinct Building 4, 6th Floor, Sheikh Zayed Road, Dubai International Financial Centre, PO Box 9275, Dubai 9275 (AE).

(81) Designated States (*unless otherwise indicated, for every kind of national protection available*): AE, AG, AL, AM, AO, AT, AU, AZ, BA, BB, BG, BH, BN, BR, BW, BY, BZ, CA, CH, CL, CN, CO, CR, CU, CZ, DE, DJ, DK, DM, DO, DZ, EC, EE, EG, ES, FI, GB, GD, GE, GH, GM, GT, HN, HR, HU, ID, IL, IN, IR, IS, JO, JP, KE, KG, KH, KN, KP, KR, KW, KZ, LA, LC, LK, LR, LS, LU, LY, MA, MD, ME, MG, MK, MN, MW, MX, MY, MZ, NA, NG, NI, NO, NZ, OM, PA, PE, PG, PH, PL, PT, QA, RO, RS, RU, RW, SA, SC, SD, SE, SG, SK, SL, ST, SV, SY, TH, TJ, TM, TN, TR, TT, TZ, UA, UG, US, UZ, VC, VN, WS, ZA, ZM, ZW.

(84) Designated States (*unless otherwise indicated, for every kind of regional protection available*): ARIPO (BW, GH, GM, KE, LR, LS, MW, MZ, NA, RW, SD, SL, ST, SZ, TZ, UG, ZM, ZW), Eurasian (AM, AZ, BY, KG, KZ, RU, TJ, TM), European (AL, AT, BE, BG, CH, CY, CZ, DE, DK, EE, ES, FI, FR, GB, GR, HR, HU, IE, IS, IT, LT, LU, LV, MC, MK, MT, NL, NO, PL, PT, RO, RS, SE, SI, SK, SM, TR), OAPI (BF, BJ, CF, CG, CI, CM, GA, GN, GQ, GW, KM, ML, MR, NE, SN, TD, TG).

(54) Title: 3D REDUCED GRAPHENE OXIDE/SIO₂ COMPOSITE FOR ICE NUCLEATION

(57) Abstract: The present invention provides for an ice-nucleating particle for cloud seeding and other applications, which can initiate ice nucleation at a temperature of -8°C. Further, the ice nucleation particle number increased continuously and rapidly with the reducing of temperature. The ice nucleating particle in the present invention is a nanostructured porous composite of 3-dimensional reduced graphene oxide and silica dioxide nanoparticles (PrGO-SN). The present invention also provides for a process for synthesizing the PrGO-SN.



WO 2020/148644 A1

3D REDUCED GRAPHENE OXIDE/SIO₂ COMPOSITE FOR ICE NUCLEATION

FIELD OF THE INVENTION

[0001] The present invention relates to the field of cloud seeding. More particularly, the present invention relates to the synthesis of 3D graphene/metal oxide nanostructured composite materials for ice nucleation in cloud seeding, artificial snow making and freeze-drying technologies in biomedical and the food industry and the like.

BACKGROUND OF THE INVENTION

[0002] The freezing of liquid water into solid ice is one of the most common natural phenomena, where ice can be formed homogeneously by pure water or heterogeneously in the presence of foreign materials called ice nucleating particles (INPs). Such INPs can originate from biological, mineralogical and anthropogenic sources, including pollen and bacteria, volcano ashes, atmospheric dust. Heterogeneous ice nucleation plays an important role in various areas, such as atmospheric physics, cryopreservation technologies, and freeze-drying in biomedical research and the food industry. For decades, although the extent to which exact properties of INPs are responsible for initiating ice nucleation and their molecular identity still remains unclear, surface properties of INPs have been considered as the main parameters that promote ice nucleating activities. A variety of mechanisms that attempt to describe the ice nucleating activities of INPs are hypothesized in the literature, most of which are focused on the discussions about the roles of INPs surface properties. For instance, previous experimental and numerical studies show that surface defects (such as cracks and cavities present in K-feldspar) as well as surface functionalization (such as hydroxyl groups present on edge sites of aluminosilicate clay minerals) may induce heterogeneous ice nucleation; the lattice match between ice and the crystalline structure of the surface can also influence the ice nucleating activities, as is the case for silver iodide (AgI), a known cold cloud seeding agent which has similar lattice constant with that of ice crystal.

[0003] The existing ice nucleation particles (INPs) used in cloud seeding applications mainly involve silver iodide (AgI), where ice nucleation occurs selectively at specific locations, such as defect sites and

lattice mismatches. It was found that defect sites are favorable locations for ice nucleation rather than perfect faces of AgI crystals. Moreover, the structures of some of the most efficient ice nucleating substances closely match the ice hexagonal lattice. However, despite its good ice nucleating ability, AgI requires much lower temperature (-25°C) to exhibit good ice-nucleating ability, in addition, it is associated with controversial environmental risk. Although there are other materials that contain favorable defect sites and similar lattice structure with ice, most of them exhibit high ice-nucleating activity only at low temperature.

[0004] Another effective INPs reported in recent years is so-called ice-active bacteria, *Pseudomonas syringae*, that is often used to facilitate artificial snow production in winter sports areas around the world. Similar to AgI, its ice-nucleating ability comes from the ice mimicry of the ice nucleation sites, which serves as a template for orienting water into a lattice. However, they only display an initial high ice nucleation counts and cannot further increase the numbers with the reduced temperature. In addition, such bacteria-based materials demand high cost for mass production and are not widely used for cloud seeding applications at present.

[0005] In addition, surface charge, surface geometry, hydrogen bonding and other surface characteristics are also hypothesized to contribute to the surface-induced ice nucleation. However, studies on ice nucleating activities of INPs are mostly limited to theoretical modelling and simulations, mainly due to the challenges in providing the suitable experimental setup, such as observation and measurement techniques that work at subzero temperature conditions, all of which have significantly restricted observation of the interaction between water vapor and the ice nucleation particles, and led to lack of information on the inception of ice nucleation and progression of ice crystal growth.

[0006] In addition to the above mentioned INPs that have been explored in the literature, various materials are also found to promote ice nucleation, among which carbon nanomaterials such as graphene and its derivatives have been investigated due to their intrinsic and functionalized surface properties. Specifically, the triangular sub lattice of graphite (2.46 Angstrom) matches the natural ice structure, which could favor the epitaxial growth of the stable hexagonal ice I_h at the atomic level.

[0007] Graphene derivatives such as graphene oxide (GO) also exhibit ice nucleating abilities because water molecules can be efficiently captured by various hydrophilic oxygen-contained functional groups

that exist on GO. Immersion droplet freezing experiments has been employed in the literature to indirectly measure the ice nucleating abilities of materials by counting the number of microscale frozen droplets, but most of the ice nucleation activities of carbon nanomaterials were only observed at relatively low temperature (usually below $-20\text{ }^{\circ}\text{C}$), which is less ideal than other ice nucleation materials such as K-feldspar and silver iodide (AgI) with higher nucleation temperature, and the real-time progress of ice growth is not captured. As a result, in situ observation of ice nucleation on these carbon nanomaterials is less known.

[0008] It has been reported that atmospheric ice particles play a crucial role in cloud formation and precipitation, and most precipitation in clouds initiates via the ice phase. Recently, studies on cloud seeding have been attracting more attentions because it is an effective method to take advantage of such water resources in clouds. Most studies focus on hygroscopic materials with high water vapor adsorbing capabilities as potential cloud seeding materials, and they are only effective at above-zero temperatures. However, studies on cloud seeding at subzero temperature (cold cloud seeding) have not seen much progress, with AgI as the most commonly used cold cloud seeding materials for decades, which is often associated with controversial environmental risk.

[0009] Use of chemicals such as silver iodide pose an ecological threat and harm to public health as silver iodide can cause temporary incapacitation or possible residual injury to humans and mammals with intense or chronic exposure. Current silver iodide micro particles used in cloud seeding have raised concerns over its toxicity in different environments; particularly aquatic environments. In addition, although the conventional method of cloud seeding has been shown to change the shape and behavior of clouds, its ability to induce rain is much uncertain. Furthermore, the structure of ice is not well understood at the nanoscale. Recent studies have proven that ice at the nanoscale has a crystalline structure that is pentagonal rather than hexagonal, opening the door for new and potentially more effective chemicals for cloud seeding.

[0010] In recent years, new formulations of seeding material are being developed for release from pyrotechnic flares (National Research Council, 2003). These materials require less AgI than older formulations, and they are much more active in ice nucleation at temperatures colder than about $-5\text{ }^{\circ}\text{C}$. Considerable work to improve the efficiency of seeding materials is being carried out by numerous

groups using complex chemical compositions, nanotechnologies, different types of cloud chambers and full-size testing stands of seeding devices. New types of cloud-seeding materials synthesized based on nanotechnologies as a promising water-augmentation technology has drawn attention. Recently there was designed and synthesized a type of core/shell NaCl/TiO₂ (CSNT) particle with controlled particle size, which successfully adsorbed more water vapor (~295 times at low relative humidity, 20% RH) than that of pure NaCl, deliquesced at a lower environmental RH of 62-66% than the hygroscopic point (hg.p., 75% RH) of NaCl, and formed larger water droplets ~6-10 times its original measured size area, whereas the pure NaCl still remained as a crystal at the same conditions. It was found that the titanium dioxide coating improved the salt's ability to adsorb and condense water vapor over 100 times compared to a pure salt crystal. Such an increase in condensation efficiency could improve a cloud's ability to produce more precipitation, making rain enhancement operations more efficient and effective. This novel material is suitable to be applied for warm cloud seeding activities.

[0011] Due to the increasing interests in cloud seeding and the limitations of the conventional cloud seeding materials there is a need in the art, to synthesize novel alternate cloud seeding materials that can increase the chance of rainfall by increasing the efficiency of rain droplet formation in the cold cloud and minimize the adverse effect on the environment. Further, there is also a need for developing ice-nucleating particles, which can initiate ice nucleation at higher temperatures.

SUMMARY OF THE INVENTION

[0012] The present invention introduces nanostructured composite materials for ice nucleation in cold cloud offering excellent in-plane and out-of-plane thermal conductivity which is in favor of ice nucleation of supercooled water. Further, the present invention provides for an ice nucleating particle which when presented in a cold atmospheric condition accelerate and enhance the formation and growth of ice crystals in mixed phase clouds. Furthermore, the present invention also provides for an ice nucleating particle, which can grow rapidly, and continuously with the constant reducing of temperature.

[0013] In an embodiment, the present invention provides for an ice nucleating composite comprising for producing a plurality of ice crystals capable of initiating ice nucleation at higher temperature of -8°C and wherein said ice crystals multiply in number when the temperature increases at or below -8°C .

[0014] In a preferred embodiment, the ice nucleating composite is a a three dimensional (3D) porous composite of reduced graphene oxide (rGO) and silicon dioxide nanoparticles, wherein the silicon dioxide nanoparticles are distributed uniformly across a hexagonal reduced graphene oxide (rGO) lattice structure. The composite of the present invention exhibits superior in -plane and out -of- plane thermal conductivity, thereby favoring favor of ice nucleation of supercooled water. wherein said particle exhibits a high water adsorption capacity of $118.86\text{ cm}^3/\text{g}$ in low humidity conditions. The composite has a high Brunauer-Emmett-Teller (BET) surface area of $178.84\text{ m}^2/\text{g}$. The higher value of $a_{s,\text{BET}}$ of the composite was attributed to the less restacking of the flexible rGO sheets during the self-assembling process, where SiO_2 nanoparticles functioned as spacers which separated the rGO sheets by occupying the interlayer gaps, caused less aggregation and therefore resulted in an increase in the surface area. Additionally, the composite has a low water contact angle of 36.2° , resulting in a higher hydrophilicity. Further, the composite comprises a plurality of pores of about 10- 100nm in size, resulting in a has a pore volume of $1.23\text{ cm}^3/\text{g}$.

[0015] In another preferred embodiment, the presne invention provides for a method of producing the ice nucleating composite. A single-step hydrothermal synthesis was carried out for the synthesis of the ice nucleating composite comprising the following steps. A graphene oxide (GO) aqueous dispersion

was prepared. Subsequently, 20 ml of ethanol (C_2H_6O), 0.7 ml ammonium hydroxide solution ($NH_3 \cdot H_2O$) and 0.7 ml of Tetraethyl orthosilicate (TEOS) were added into the 15 ml of graphene oxide solution to form a homogeneous mixture. The mixture was sonicated for 30 minutes then transferred into a sealed Teflon-lined autoclave and heated hydrothermally at 180 °C for 12 hours. Under sonication, silica nanoparticles were formed via Stöber process, where TEOS was hydrolyzed in alcohol in the presence of $NH_3 \cdot H_2O$ as a catalyst. The synthesized SiO_2 nanoparticles became attached to the GO sheets in the dispersion by forming hydrogen bonds with oxygen-containing groups on GO sheets. The mixture then underwent self-assembly in a hydrothermal process to form a black-colored sponge-like structure of 3-dimensional reduced graphene oxide and silica dioxide nanoparticles (PrGO-SN). After hydrothermal process, formed PrGO-SN composite was washed with deionized water (DI) water three times. The washed PrGO-SN composite was then put into a freezer at -20 °C overnight and subsequently, the PrGO-SN composite was transferred into freeze dryer at -100 °C for 24 hours.

BRIEF DESCRIPTION OF THE DRAWINGS

[0016] The subject matter that is regarded as the invention is particularly pointed out and distinctly claimed in the claims at the conclusion of the specification. The foregoing and other aspects, features, and advantages of the invention are apparent from the following detailed description taken in conjunction with the accompanying drawings in which-

[0017] FIG. 1A illustrates a schematic representation of the PrGO-SN composite porous structure that adsorbs and condenses water thereby triggering ice growth from the pores in accordance with an embodiment of the present invention;

[0018] Fig. 1B depicts the ice nucleation mechanism of the PrGO-SN composite in accordance with an embodiment of the present invention;

[0019] Fig. 2 illustrates a schematic flowchart for the synthesis of PrGO-SN in accordance with an embodiment of the present invention;

[0020] Fig. 3 graphically depicts a comparison of water vapor adsorption capacity of different PrGO-SN composites in accordance with an embodiment of the present invention;

[0021] Fig. 4A depicts the SEM image of the rGO sheet in accordance with an embodiment of the present invention;

[0022] Fig. 4B depicts the SEM image of the PrGO-SN composite where SiO₂ nanoparticles were enveloped within the 3D rGO network in accordance with an embodiment of the present invention;

[0023] Fig. 4C depicts the SEM image of the PrGO-SN composite where SiO₂ nanoparticles were enveloped within the 3D rGO network, when the scale bar is 200nm in accordance with an embodiment of the present invention;

[0024] Fig. 4D depicts the TEM image of the PrGO-SN composite in accordance with an embodiment of the present invention;

[0025] Fig. 4E depicts the structure of SiO₂ nanoparticles in accordance with an embodiment of the present invention;

[0026] Fig. 4F depicts the FTIR spectra of rGO, SiO₂ and the PrGO-SN composite, respectively in accordance with an embodiment of the present invention;

[0027] Fig. 5 graphically depicts the Simultaneous thermal analysis (STA) of the relative mass ratio of the PrGO-SN composite in accordance with an embodiment of the present invention;

[0028] Fig. 6A depicts the pore size distribution of PrGO-SN composite and rGO based on the Barrett-Joyner-Halenda method in accordance with an embodiment of the present invention;

[0029] Fig. 6B depicts the specific surface area ($a_{s,BET}$) of rGO and the PrGO-SN composite based on the Brunauer-Emmet-Teller method using N₂ adsorption/desorption isotherm in accordance with an embodiment of the present invention;

[0030] Fig. 6C depicts a water vapor adsorption isotherm of rGO and the PrGO-SN at relative humidity ranging from 60 % to 75 % in accordance with an embodiment of the present invention;

[0031] Fig. 6D depicts the water contact angle measurement of the PrGO-SN composite and AgI particles, respectively in accordance with an embodiment of the present invention;

[0032] Fig. 7A depicts the ice nucleation activities of the PrGO-SN composite observed by E-SEM experiments under controlled temperature and water vapor pressure conditions in form of hexagonal ice crystals in accordance with an embodiment of the present invention;

[0033] Fig. 7B depicts the ice nucleation activities of the PrGO-SN composite observed by E-SEM experiments under controlled temperature and water vapor pressure conditions in form of bulk ice in accordance with an embodiment of the present invention;

[0034] Fig. 7C depicts the different ice formation patterns in the rough region with cavities in accordance with an embodiment of the present invention;

[0035] Fig. 7D depicts the different ice formation patterns in the smooth region in accordance with an embodiment of the present invention;

[0036] Figs. 8A- 8C shows additional E-SEM images of showed different ice formation patterns of of the PrGO-SN composite in rough region with cavities in accordance with an embodiment of the present invention; and

[0037] Figs. 8D- 8F shows additional E-SEM images of showed different ice formation patterns of of the PrGO-SN composite in the smooth region in accordance with an embodiment of the present invention.

DETAILED DESCRIPTION OF THE INVENTION

[0038] The aspects of the ice nucleating particle of the present invention will be described in conjunction with Figures 1 – 8. In the Detailed Description, reference is made to the accompanying figures, which form a part hereof, and in which is shown by way of illustration specific embodiments in which the invention may be practiced. It is to be understood that other embodiments may be utilized and logical changes may be made without departing from the scope of the present invention. The following detailed description, therefore, is not to be taken in a limiting sense, and the scope of the present invention is defined by the appended claims.

[0039] The present invention introduces nanostructured composite materials for ice nucleation in cold cloud offering excellent in-plane and out-of-plane thermal conductivity which is in favor of ice nucleation of supercooled water. Further, the present invention provides for an ice nucleating particle which when presented in a cold atmospheric condition catalyze and enhance the formation and growth of ice crystals in mixed phase clouds. Furthermore, the present invention also provides for an ice nucleating particle, which can grow rapidly, and continuously with the constant reducing of temperature.

[0040] The present invention focusses at designing and synthesizing novel ice nucleating particles for ice nucleation in cold cloud. The invention introduces a porous composite of 3-dimensional (3D) reduced graphene oxide (rGO) and silica dioxide nanoparticles (PrGO-SN) aiming to initiate ice nucleation at higher temperature as well as sustained rapid ice crystal growth.

[0041] In an embodiment of the present invention, an interconnected 3D composite structure of PrGO-SN with narrow-sized SiO₂ nanoparticles uniformly distributed across the entire rGO structure is produced via a single-step hydrothermal process. This composite promotes enhanced ice nucleation at relatively warm temperature with high ice nucleating activities based on the following hypothesis: 3D-rGO provided templates that facilitated ice crystal growth due to its hexagonal lattice structure; SiO₂ nanoparticles enhanced the overall water molecule adsorption capabilities of the PrGO-SN composite and enabled less aggregation of the overall 3D-rGO structure, thus leading to more available sites for ice nucleation as illustrated in Fig. 1A and Fig. 1B.

[0042] Fig.1 A illustrates a schematic representation of the PrGO-SN composite porous structure that adsorbs and condenses water thereby triggering ice growth from the pores. Fig. 1B depicts the ice nucleation mechanism of the PrGO-SN composite.

[0043] Theoretical consideration of the enhanced ice formation mechanism:

[0044] Ice formation involves the processes of nucleation and growth. In the context of heterogeneous ice nucleation, water molecules start to form ice crystal seeds on the surface of INPs, and there are many factors that can influence the performance of ice nucleation. Numerous studies have been trying to analyze the rate of ice nucleation using various fundamental theories, one of which is classical nucleation theory (CNT), a simplified theoretical approach that describes that ice nucleation process. As Eq. 1 shows, the nucleation rate per unit volume J is mainly attributed to the properties of the INPs, including ρ_I , the number density of sites for heterogeneous nucleation, Z_j , the rate at which a nucleus overcomes the energy barrier and grows into a new phase (also known as Zeldovich factor which depends on $\Delta\varphi^*$ the formation energy of the critical cluster and N^* the number of molecules in the cluster), and ΔF^* , the free energy cost of creating the critical nucleus (ΔF^* depends on θ the contact angle and ξ the geometry of the INPs). Other parameters present in Eq. 1 are k the Boltzmann constant and T the temperature.

$$J = \rho_I Z_j * \exp\left(-\frac{\Delta F^*}{kT}\right), \quad Z_j = \sqrt{\frac{\Delta\varphi^*}{3\pi kT(N^*)^2}}, \quad \Delta F^* = \Delta F_{HOMO}^* * f(\theta, \xi) \quad (1)$$

[0045] Ice nucleation involves ordering of the water molecules that are rearranged into their favored lattice positions, such as the most common hexagonal ice crystals (I_h) where water molecules arranged in layers of hexagonal rings. If the molecular geometry and chemistry of the INP surface is compatible with ice (such as lattice match), then an ice embryo formed on such surface within the liquid phase will have a lower free energy than an independent ice embryo and its growth will be facilitated. Therefore, an efficient nucleating surface would have low free energy of the interface which it forms with ice, which is consistent with Eq. 1 where smaller value of ΔF^* leads to larger J .

[0046] The present invention aims to design and introduce a porous composite of 3-dimensional (3D) reduced graphene oxide (rGO) and silica dioxide nanoparticles (PrGO-SN) composite such that the

surface of 3D-rGO serves as a template for ice crystal growth due to its hexagonal lattice structure (ΔF^* lowering). Further, the presence of SiO₂ nanoparticles in the PrGO-SN at the interlayer gaps between rGO sheets allows less aggregation of the overall 3D-rGO structure, thus leading to more available sites for ice nucleation (ρ_I increasing); more importantly, the hydrophilicity of SiO₂ nanoparticles also facilitates the collection of water molecules on the rGO surface, which could facilitate sufficient water molecules for sustained rapid growth of ice crystals (θ lowering). In addition, it is reported that the minimum number of water molecules are necessary for ice nucleation to form a complete icosahedral symmetry of hexagonal geometry, thus more water molecules that are collected by the hydrophilic SiO₂ nanoparticles can speed up the onset of ice nucleation and growth. Hence, both components of the PrGO-SN composite have a collective effect of enhancing the ice nucleation rate J .

[0047] Besides, the porous structure of the PrGO-SN composite of the present invention also enables liquid water condensation in these pores even below saturation by the inverse Kelvin effect. As Eq. 2 shows, the relative humidity with respect to water (RH_w) for a pore to fill is predicted by the Kelvin effect with a negative sign to account for the concave nature of the meniscus:

$$\ln\left(\frac{P_0}{P}\right) = -\frac{4\gamma \cos(\theta)V_l}{DRT} \quad (2)$$

[0048] Where $\frac{P_0}{P}$ denotes the saturation ratio with respect to water, γ is the surface tension of water-vapor interface, V_l is the molar volume of water, D is the pore diameter, θ is the contact angle of water on the material, R is the gas constant and T is the temperature in Kelvin. Eq. 2 indicates that the narrower the pore width (smaller pore size), the lower the RH_w required for pore condensation to occur. Conversely, the higher the contact angle of water on the material, the higher the RH_w needed for pore filling. On top of the inverse Kelvin effect, the structure and composition of the PrGO-SN composite implied that the hydrophilicity of SiO₂ nanoparticles can facilitate the collection of water molecules, and subsequently water molecules can reorganize in hexagonal structure on the rGO surface, which eventually leads to ice nucleation at suitable temperature.

[0049] On the other hand, since hydrogen bonds break and reform constantly depending on the thermal fluctuation of the water molecules, the balance between water-water and water-surface interactions is crucial for ice nucleation events, that is, if one type of interactions dominates the other, ice nucleation

would not be favored because it would be either too volatile or too stable to trigger ice nucleation. Hence, surface properties are key to enabling and stabilizing ice nucleation. It is noteworthy that the balance between water-water and water-surface interactions is partly influenced by the quantity of water molecules around the PrGO-SN composite; if the quantity is high, then the water-water interaction will be stronger than the water-surface interaction, which would be difficult for water molecules to reorganize into hexagonal structure and form ice. This is supported by the study that the ice nucleation can be enhanced by a huge factor of 10 at the air-water interface than water-water interface. Since SiO₂ nanoparticles can capture water vapor due to high water vapor adsorption capabilities and form a thin layer of liquid water on the PrGO-SN composite, there will exist a liquid/solid interface that has a positive bridging effect between water vapor and the solid surface of the composite. Ice nucleation will initiate from the thin water layer and the ice will grow at the expense of the water vapor in air.

[0050] Synthesis of the PrGO-SN composite:

[0051] The synthesis of PrGO-SN of the present invention is illustrated in Figure 2. A single-step hydrothermal synthesis was carried out for the synthesis with following details. A GO aqueous dispersion was prepared using the improved Hummers method. 15 ml of GO solution (2 mg/ml concentration) as prepared above (using the Hummers method) was then mixed with 20 ml of ethanol (C₂H₆O). Subsequently, 0.7 ml ammonium hydroxide solution (NH₃•H₂O) and 0.7 ml and 1.4 ml of Tetraethyl orthosilicate (TEOS) were added into the mixture respectively to prepare 2 separate samples. The mixtures are sonicated for 30 minutes then transferred into a sealed Teflon-lined autoclave and heated hydrothermally at 180 °C for 12 hours. Under sonication, silica nanoparticles were formed via Stöber process, where TEOS was hydrolyzed in alcohol in the presence of NH₃•H₂O as a catalyst. The synthesized SiO₂ nanoparticles became attached to the GO sheets in the dispersion by forming hydrogen bonds with oxygen-containing groups on GO sheets. The mixture then underwent self-assembly in a hydrothermal process to form a black-colored sponge-like structure of 3-dimensional reduced graphene oxide and silica dioxide nanoparticles (PrGO-SN). After hydrothermal process, formed PrGO-SN composite was washed with deionized water (DI) water three times. The washed PrGO-SN composite was then put into a freezer at -20 °C overnight and subsequently, the PrGO-SN composite was transferred into freeze dryer at -100 °C for 24 hours. The ice nucleation performance of the PrGO-SN

composite was further determined through in-situ visual observation by Environmental - Scanning Electron Microscope (E- SEM).

[0052] Characterization and Measurements:

[0053] The synthesized PrGO-SN composite was characterized through Scanning Electron Microscopy (SEM, Quanta 250, FEI Company); Transmission Electron Microscopy (TEM, Tecnai from FEI™ Company operating at 200 KV); A Fourier transform infrared Nicolet iS10 spectrometer (FTIR, Thermo Fisher Scientific, Inc.). Water static-contact-angle Measurements (Kyowa DM-701) elaborated with an interface Measurement & Analyses System and the droplets of 0.8 µl. The water vapor adsorption performance of the PrGO-SN composite was determined quantitatively via a water-vapor adsorption isotherm test (Brunauer-Emmett-Teller, Belsorb Max, Japan) in water-vapor mode. The samples were pretreated at 100 °C for 3 hours under a pressure $< 10^{-4}$ Pa before commencing the water vapor adsorption isotherm analysis and the whole test required 24 hours. Environmental scanning electron microscopy (E-SEM) was used for in-situ observation of the ice nucleation activities of the PrGO-SN composite. The water vapor adsorption isotherm analysis confirmed that PrGO-SN sample prepared by 0.7 ml of TEOS had higher water vapor adsorption capacity as shown in Fig. 3.

[0054] Fig. 3 illustrates a comparison of water vapor adsorption capacity of different PrGO-SN composites. It can be seen from the graph shown in Fig. 3 that at low relative humidity conditions ranging from 60 % to 75 %, the adsorbed water-vapor volume of the PrGO-SN (0.7ml TEOS) sample was higher than that of the PrGO-SN(1.4ml TEOS) sample; as the relative humidity increases, the difference in water vapor adsorption capacity was even larger.

[0055] The 3D-rGO/MO materials produced in this invention, when evaluated by micro-scale ice nucleation measurement, show that 3DrGO/SiO₂ produced can initiate ice nucleation at -8°C which is higher temperature than most previous reported materials such as AgI and feldspar. Further, the ice nucleation particle number increased continuously and rapidly with the reducing of temperature.

[0056] Surface morphology of rGO and the cross-sectional image of the PrGO-SN:

[0057] The microscopic surface morphology of rGO and the cross-sectional image of the PrGO-SN composite are shown in Figs. 4A to 4E. When the GO dispersion underwent hydrothermal process as mentioned above, a well-connected 3D porous structure was formed with many interconnected rGO

sheets as shown in Fig. 4A. As for the PrGO-SN composite, the SEM image confirmed that SiO₂ nanoparticles were homogeneously embedded in rGO and distributed across almost the entire rGO network as shown in Fig. 4B. The internal structure of the PrGO-SN composite also revealed the overall distribution of SiO₂ nanoparticles enveloped within the 3D-rGO network. Further observations under TEM suggested that SiO₂ nanoparticles occupied the interlayer gaps between rGO sheets, indicating that the SiO₂ nanoparticles played a spacer role in separating the rGO sheets and thus resulted in less aggregation compared to the pristine rGO. Fig. 4D shows different contrasts of rGO sheets and SiO₂ nanoparticles, which indicated the co-existence of SiO₂ nanoparticles and rGO layers. In addition, it can be found that SiO₂ nanoparticles presented in spherical structure with an average size of 10-20 nm as shown in Fig. 4E.

[0058] Furthermore, Simultaneous Thermal Analysis (STA) was conducted to determine the composition of each component in the PrGO-SN composite, and the result indicated that the mass percentage of rGO in the PrGO-SN composite is about 18 wt% as shown in Fig.5. Fig. 5, depicts the Simultaneous thermal analysis (STA) of the relative mass ratio of the PrGO-SN composite. It is indicated in Fig. 5 that rGO accounted for 18 % of the total composite mass. Typically, the mass of composite did not change much until 500 °C. Before 500 °C, most of the mass loss was due to the evaporation of water molecules inside the composite; after 500 °C, carbonaceous materials started to burn, resulting in significant mass loss.

[0059] The functional groups of each component of the PrGO-SN composite were confirmed by FTIR (Fourier transform infrared Nicolet iS10 spectrometer) as shown in Fig. 4F. Peaks of C=C, C-O and Si-O-Si from the composite sample confirmed the presence of both rGO and SiO₂ nanoparticles. Moreover, the relatively strong peak of the composite at 1060~1075 cm⁻¹ corresponds to the superimposition between the C-O and Si-O-Si peaks. The peaks of -OH and O-H were barely visible (Fig. 3F), implying that most of the oxygen-containing groups were removed during the hydrothermal reaction process. The slightly stronger -OH signal from the PrGO-SN composite than the rGO could result from the presence of silanol groups that normally associated with SiO₂ nanoparticles.

[0060] The pore size distribution and total pore volume of both the PrGO-SN composite and rGO were determined by the Barrett-Joyner-Halenda (BJH) method. As Fig. 6A shows, BJH result demonstrated

that the PrGO-SN composite had significantly more pores of size range between 10–100 nm and peaked at around 50 nm compared to rGO which had less pores of larger sizes, suggesting that the co-existence of SiO₂ nanoparticles and 3D-GO framework contributed to the formation of smaller pores (10-100nm) in the composite structure. In addition, the PrGO-SN composite has a total pore volume (V_p) of 1.23 cm³/g, compared to that of rGO 0.69 cm³/g. This BJH result indicated that the porosity of the PrGO-SN composite has been greatly increased compared to the rGO. The specific surface area ($a_{s,BET}$) of the rGO and the PrGO-SN composite were determined by the Brunauer-Emmet-Teller (BET) method using N₂ adsorption/desorption isotherms with 167.31 m²/g for rGO and 178.84 m²/g for the composite, respectively as shown in Fig. 6B. The higher value of $a_{s,BET}$ of the composite was attributed to the less restacking of the flexible rGO sheets during the self-assembling process, where SiO₂ nanoparticles functioned as spacers which separated the rGO sheets by occupying the interlayer gaps, caused less aggregation and therefore resulted in an increase in the surface area.

[0061] Water-vapor adsorption isotherm analysis was conducted to quantitatively determine the water-vapor adsorption capacity of the PrGO-SN composite compared to the rGO. It was found that, even at low relative humidity conditions ranging from 60 % to 75 %, the adsorbed water-vapor volume of the composite was higher than that of the rGO [118.86 cm³/g compared with that (105.95 cm³/g) of rGO at 75 % RH], which enabled the composite to adsorb more water vapor that potentially contributed to ice nucleation at suitable temperature as shown in Fig. 6C. Although both PrGO-SN composite and rGO demonstrated good water vapor adsorption capacity, it can be inferred that the PrGO-SN composite could adsorb much more water vapor than the rGO at higher RH value. This feature was attributed to both the hydrophilicity of SiO₂ nanoparticles and the porous structure of the PrGO-SN composite. Further, the water contact angle of the PrGO-SN composite was determined by deionized water static-contact-angle measurements. The PrGO-SN powder sample was pressed into a plate form through compression molding method, and the measured contact angle of the plate sample was used as approximation for the actual PrGO-SN composite particles. As shown in Fig. 6D, the contact angle of the PrGO-SN composite is as low as 36.2°, thereby confirming its strong hydrophilic property. A low contact angle can lead to higher ice nucleation activities because of the lowering of free energy cost of creating the critical nucleus thereby increasing the water vapor adsorption performance. In comparison,

the contact angle of silver iodide (AgI) particles for example, is 131.1° , which shows strong hydrophobic property. Based on the above results and comparisons, PrGO-SN composite sample of the present invention has demonstrated the structure and property of a nanostructured porous materials with higher water vapor adsorption capacity, higher BET specific surface area and lower water contact angles (i.e. more hydrophilic). Such characteristics of PrGO-SN composite are in favor of initiating ice nucleation at an extremely lower critical temperature and vapor pressure in addition to rapid ice crystal growth.

[0062] Observation of ice nucleating on PrGO-SN composites:

[0063] Environmental scanning electron microscopy (E-SEM) was employed for in-situ observation of the ice nucleation activities of the PrGO-SN composite. For all E-SEM experiments, the supersaturated relative humidity conditions and the sub-zero temperature for the first occurrence of ice nucleation and the subsequent growth were controlled by adjusting the partial pressure of water vapor as well as the temperature in the chamber. Firstly, samples were pretreated in the chamber for 60 min with the temperature of the chamber set at -8°C and the relative humidity (RH) at $\sim 80\%$. This pretreatment allows for stabilizing the temperature and relative humidity conditions. Secondly, RH in the chamber was gradually increased at a constant rate ($\sim 5\text{ Pa/s}$) until first ice nucleation events were observed, and the RH stopped increasing and was kept constant; meanwhile ice crystal growth progressed rapidly at this RH value. Multiple experiments were performed under such procedures and it was found that the RH value at which first nucleation event was observed ranged from 5% to 8% supersaturation. Same procedures were followed at even higher temperature of -7 and -6°C , but no ice nucleation events were observed regardless of the increase in RH. Therefore, -8°C was determined as the highest and optimal ice nucleation temperature for the PrGO-SN composite. It is noteworthy that no water droplet was found at any stage throughout the E-SEM experiments, indicating that the water vapor was transformed directly into ice crystals.

[0064] E-SEM experiments showed that, under the same conditions, PrGO-SN composite-induced ice nucleation resulted in two different appearances of ice crystals: 1) those that tended to grow into individual hexagonal crystals; and 2) those merging with each other and forming bulk ice, as depicted in Fig. 7A and 7B respectively. This phenomenon suggested that different surface features of the PrGO-

SN composite may have different influence on ice nucleation and growth. To further analyze such phenomenon, regions of the PrGO-SN composite with different morphologies were carefully observed by E-SEM observation: one with apparent topographic roughness such as large cavities on the surface, the other with relatively smooth surface absent of large cavities, as shown in Fig. 7C and Fig. 7D, respectively.

[0065] As shown in Fig. 7C, when RH reached ~5% supersaturation, first ice nucleation event took place on the sample regions with large cavities and then started to grow within ~10 s from the beginning of the experiment (c2). When RH increased to ~8% supersaturation and ~20 s into the experiment, ice crystals grew larger and displayed visible hexagonal shape in the cavity of the sample (c3). In comparison, Fig. 7D shows that ice nucleation was only observed on the sample regions with smooth surface until the conditions reached ~8% supersaturation and ~30 s from the beginning of the experiment (d2). However, in the later sample, once the ice crystals were formed, spontaneous ice growth occurred and ice crystals covered almost the entire surface of the sample within a short period of time (only ~5 s) from the first ice nucleation event (d3). It is noteworthy that for both scenarios, the nucleated ice crystals can sustain their growth at constant RH.

[0066] Further, multiple E-SEM ice nucleation experiments were conducted, and more SEM images of ice nucleation events in rough region with cavities as shown in Figs. 8A- 8C; and relatively smooth region as shown in Figs 8D – 8F respectively. As it can be seen from Figs 8A- 8C, the E-SEM experiments showed different ice formation patterns in rough region with the presence of cavities. Alternatively, it can be seen from Figs. 8D- 8F the ice formation patterns in the smooth region is in form of hexagonal ice crystals and bulk ice.

[0067] It can be found that for the rough sample regions with large cavities, ice nucleation could be incepted on such large cavities and grown into hexagonal shape ice crystals (Fig. 7C). In the case of sample with relatively smooth regions, simultaneous ice nucleation occurred at multiple sites, and the formed ice crystals tended to merge and form large chunks of ice as can be seen from Fig. 7D. The differences in ice crystal growth behaviors were affected by the regions with different surface roughness. In general, topographic roughness on the PrGO-SN composite tended to favor condensations of vapor into liquid. Specifically, in the case of porous composite of PrGO-SN, rough regions with

larger surface areas possess cavities and more small pores than relatively smooth regions. As a result, condensed water vapor would be accumulated first in the cavities on the PrGO-SN composite, thus these locations would have higher ice nucleation activities due to the confined nucleation sites and sufficient water vapor uptake. On the other hand, relatively smooth PrGO-SN region tended to adsorb water vapor more homogeneously, thus ice nucleation tended to occur at multiple sites simultaneously; however, due to the competition of condensed water vapor among the neighboring sites, ice nucleation would take longer time to be observed visually. Once the ice nucleation event occurred at multiple sites, the formed small ice crystals would quickly merge together to form bulk ice). By observing the ice nucleating on PrGO-SN composites using the temperature/water-vapor-pressure controlled E-SEM, it was founded that the porous composite of PrGO-SN demonstrated the initiation of ice nucleation at higher temperature as well as continuous rapid ice crystal growth, which showed potential as a promising candidate for ice nucleation materials.

[0068] The 3DrGO/SiO₂ produced in the present invention exhibit various advantages over standard ice nucleating materials. First advantage is the 3D reduced graphene oxide framework offers excellent in plane and out-of-plane thermal conductivity, which is in favor of ice nucleation of super cooled water. Second advantage is the highly porous and hydrophilic SiO₂ nanoparticle contribute in adsorbing the free-moving water molecules and assisting in achieving the fixed and packed orientation of water molecules in order to form the ice. Both positive factors possessed by the 3D-rGO/SiO₂ have not been achieved by standard ice nucleating particles.

[0069] The present invention aims at designing a nanostructured porous composite of 3-dimensional reduced graphene oxide and silica dioxide nanoparticles (PrGO-SN). An interconnected 3D composite structure of PrGO-SN with narrow-sized SiO₂ nanoparticles uniformly distributed across the entire rGO structure was produced via controlled single-step hydrothermal process. The PrGO-SN composite not only offered hexagonal ice crystal growth via lattice match between the ice and crystalline structure of the substrate that may induce heterogeneous ice nucleation from its 3D rGO component, but also provided high Brunauer-Emmett-Teller (BET) surface area and water vapor adsorption capacity. In addition, PrGO-SN composite has good porosity and more hydrophilic surface from its SiO₂ nanoparticles component which were all suitable factors to promote ice nucleation and growth. In – situ

observations via an Environmental-Scanning Electron Microscope (E-SEM) confirmed the enhanced ice nucleation performance of the PrGO-SN composite evidenced by visible ice nucleation event starting from -8 °C, 5- 8% RH supersaturation. In addition, it was founded that ice nucleation was incepted on large cavities in the rougher region of the PrGO-SN composite sample and grew into hexagonal shape ice crystals. Alternatively, ice nucleation event occurred simultaneously at multiple sites in a smoother region of the sample, then merged rapidly together to form bulk ice. By observing the ice nucleating on PrGO-SN composites under E-SEM, it was confirmed that the porous composite of PrGO-SN demonstrated the initiation of ice nucleation at higher temperature as well as continuous rapid ice crystal growth.

[0070] Many changes, modifications, variations and other uses and applications of the subject invention will become apparent to those skilled in the art after considering this specification and the accompanying drawings, which disclose the preferred embodiments thereof. All such changes, modifications, variations and other uses and applications, which do not depart from the spirit and scope of the invention, are deemed to be covered by the invention, which is to be limited only by the claims, which follow.

CLAIMS

- 1) An ice nucleating composite for producing a plurality of ice crystals, wherein said composite initiates ice nucleation at a temperature of -8°C ; and wherein said composite multiplies the ice crystals in number when the temperature increases at or below -8°C .
- 2) The ice nucleating composite as claimed in claim 1, wherein said composite is a porous nanostructured composite material of graphene metal oxide.
- 3) The ice nucleating composite as claimed in any one of claims 1 or 2, wherein said composite is a porous composite of reduced graphene oxide (rGO) and silicon dioxide nanoparticles.
- 4) The ice nucleating composite as claimed in any one of claims 1 to 3, wherein said composite is a three dimensional (3D) porous composite of reduced graphene oxide (rGO) and silicon dioxide nanoparticles.
- 5) The ice nucleating composite as claimed in any one of claims 1 to 4, wherein the silicon dioxide nanoparticles are distributed uniformly across a hexagonal reduced graphene oxide (rGO) lattice micro-structure.
- 6) The ice nucleating composite as claimed in any one of claims 1 to 3, wherein said composite exhibits a high water adsorption capacity of $118.86\text{ cm}^3/\text{g}$ in low humidity conditions.
- 7) The ice nucleating composite as claimed in any one of claims 1 to 3, wherein said composite has a Brunauer-Emmett-Teller (BET) surface area, for example $178.84\text{ m}^2/\text{g}$.

- 8) The ice nucleating composite as claimed in any one of claims 1 to 3, wherein said composite has a low water contact angle, for example 36.2° and higher hydrophilicity.
- 9) The ice nucleating composite as claimed in any one of claims 1 to 3, wherein said composite comprises a plurality of pores of about 10- 100nm in size.
- 10) The ice nucleating composite as claimed in any one of claims 1 to 3, wherein said composite has a high pore volume, for example $1.23 \text{ cm}^3/\text{g}$.
- 11) A process for preparing the ice nucleating composite as claimed in claim 1, the process comprising the steps of:
 - preparing an aqueous dispersed graphene oxide solution;
 - adding the aqueous solution of graphene oxide to ethanol, ammonium hydroxide and tetraethyl orthosilicate forming a homogenous mixture;
 - sonicating the homogenous mixture to obtain a sonicated mixture;
 - heating the sonicated mixture in an autoclave thus obtaining the ice nucleating composite;
 - rinsing the ice nucleating composite with a deionised water; and
 - freeze-drying the composite to preserve the 3D micro-structure.
- 12) The process for preparing the ice nucleating composite as claimed in claim 11, wherein the concentration of graphene oxide solution was 2 mg/ml.
- 13) The process for preparing the ice nucleating composite as claimed in claim 11, wherein 20 ml of ethanol was added to the aqueous solution of graphene oxide.
- 14) The process for preparing the ice nucleating composite as claimed in claim 11, wherein 0.7 ml of ammonium hydroxide was added to the aqueous solution of graphene oxide, other volume may apply.

- 15) The process for preparing the ice nucleating composite as claimed in claim 11, wherein 0.7 ml of tetraethyl orthosilicate was added to the aqueous solution of graphene oxide, other volume may apply.
- 16) The process for preparing the ice nucleating composite as claimed in claim 11, wherein the homogenous mixture comprising the aqueous solution of graphene oxide, ethanol, ammonium hydroxide and tetraethyl orthosilicate is sonicated at room temperature for at least 30 minutes.
- 17) The process for preparing the ice nucleating composite as claimed in claim 11, wherein the sonicated mixture is heated in a Teflon lined autoclave.
- 18) The process for preparing the ice nucleating composite as claimed in claim 11, wherein the sonicated mixture is heated at 180°C for at least 12 hours.
- 19) The process for preparing the ice nucleating composite as claimed in claim 11, wherein the ice nucleating composite is washed with deionised water at least three times.
- 20) The process for preparing the ice nucleating composite as claimed in claim 11, wherein the ice nucleating composite is frozen in a freeze dryer at -100°C for at least 24 hours.

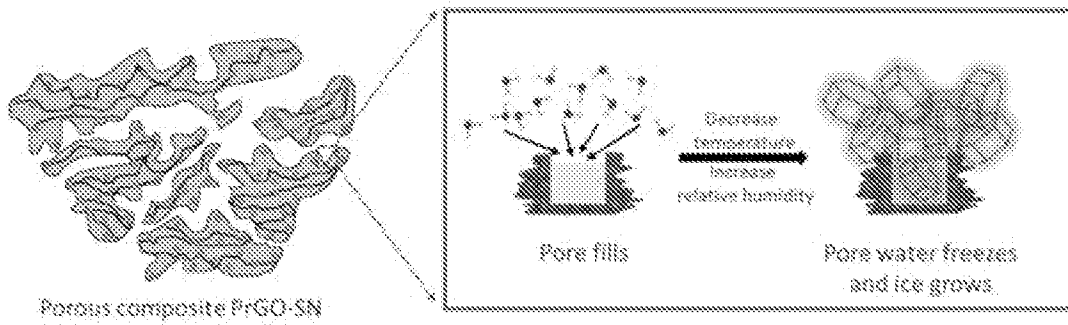


FIG. 1A

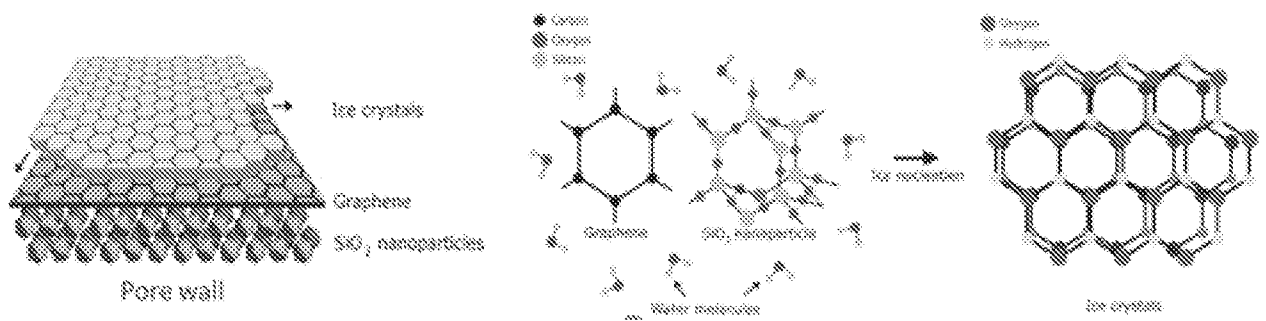


FIG. 1B

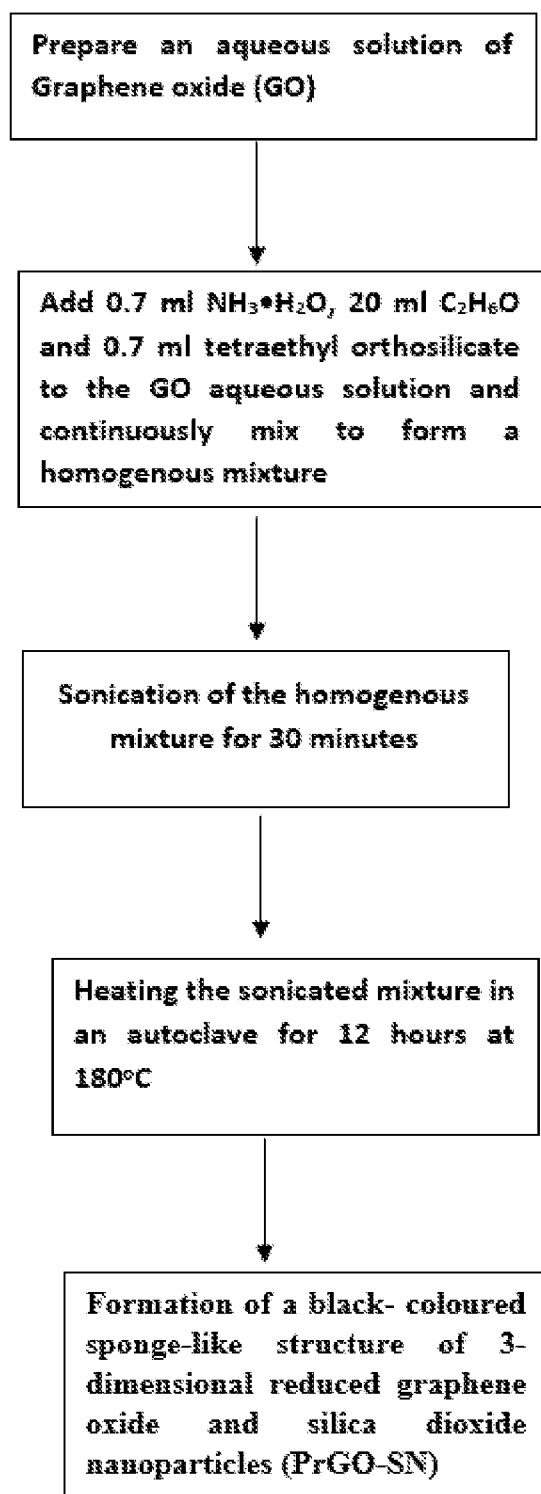


FIG. 2

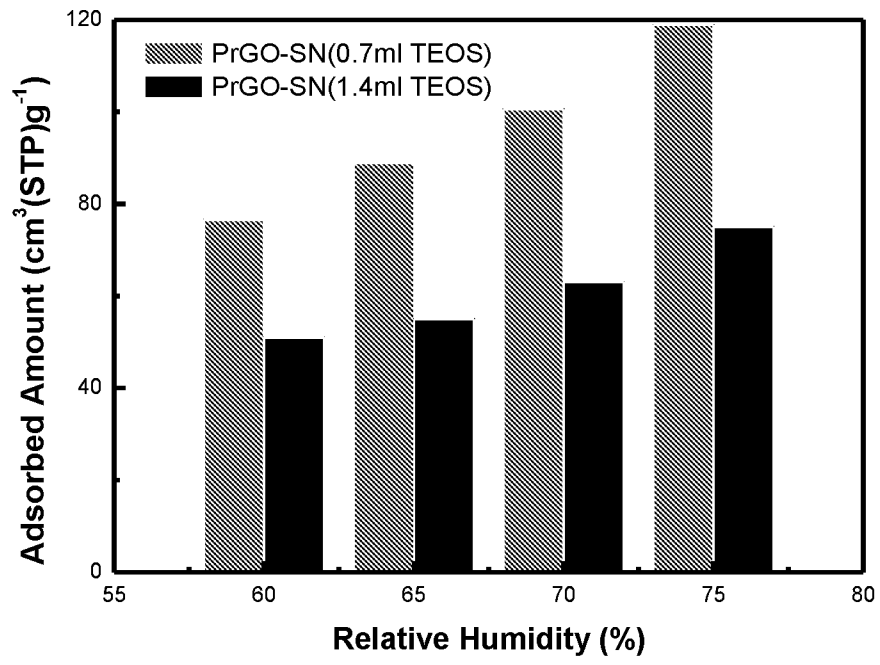


FIG.3

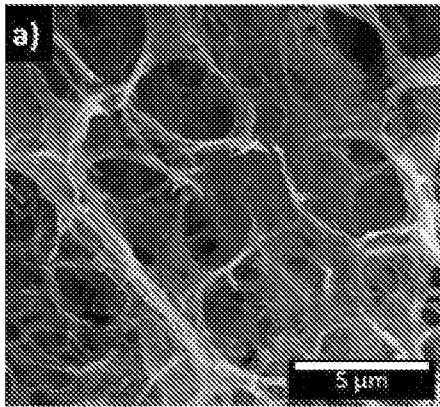


FIG. 4A

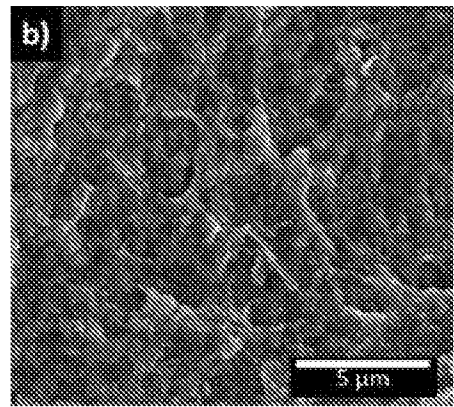


FIG. 4B

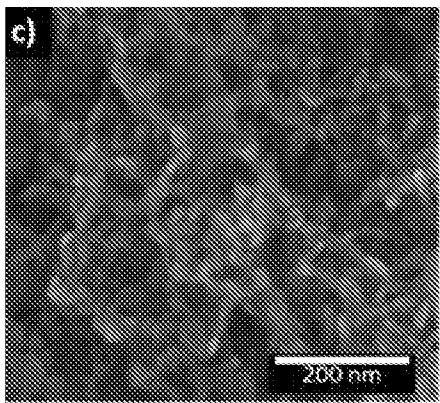


FIG. 4C

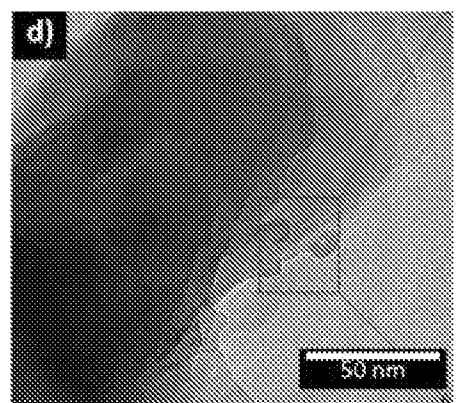


FIG. 4D

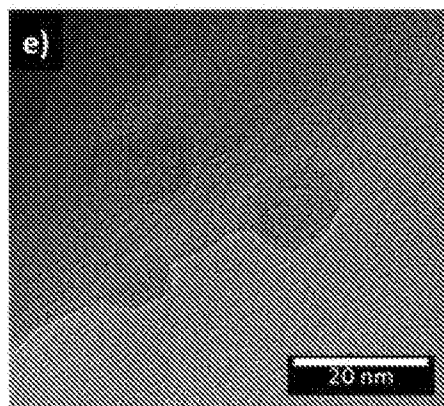


FIG. 4E

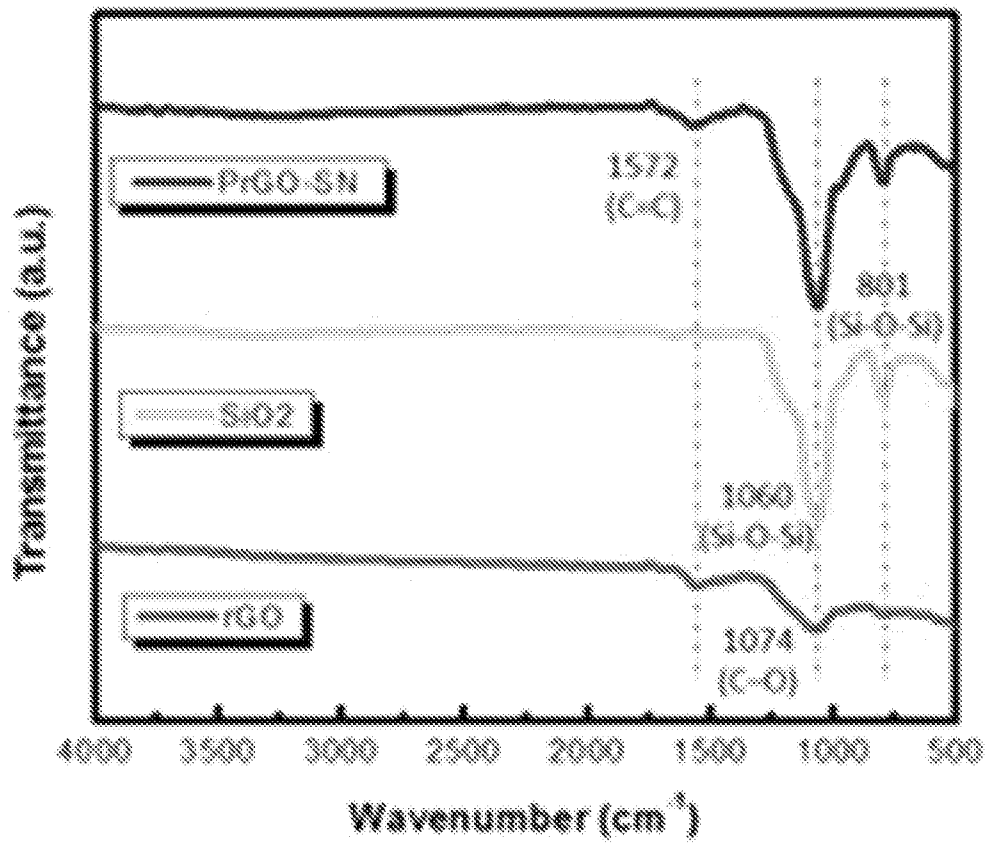


FIG. 4F

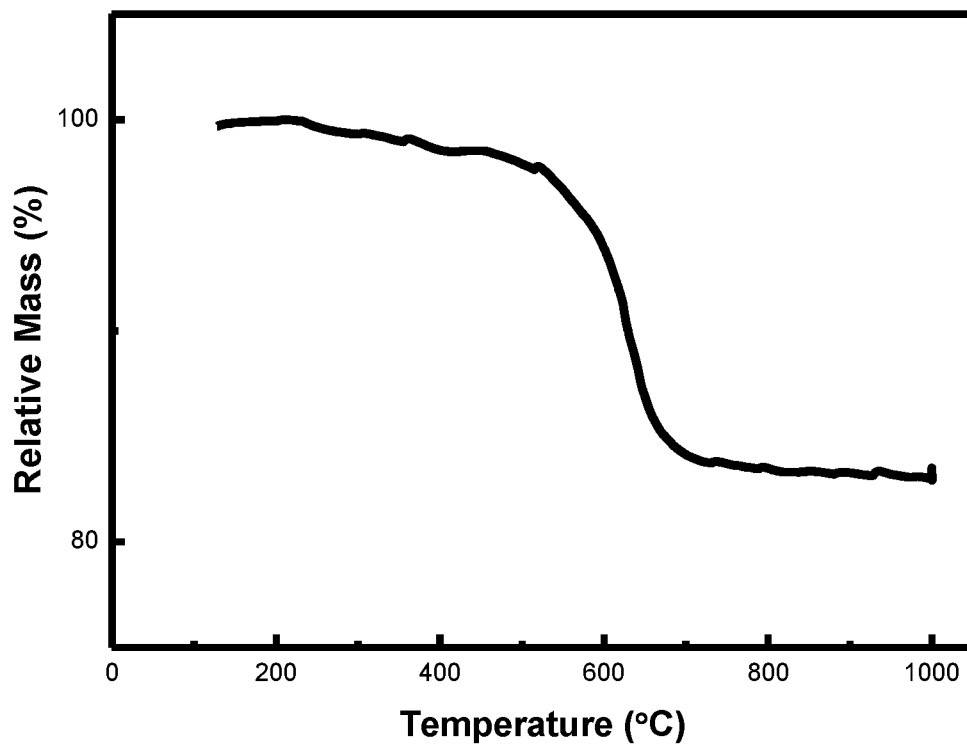


FIG. 5

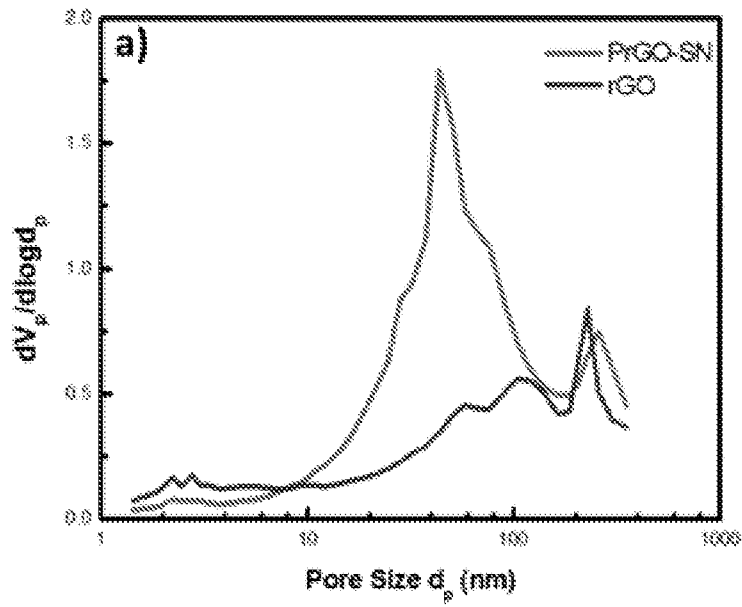


FIG. 6A

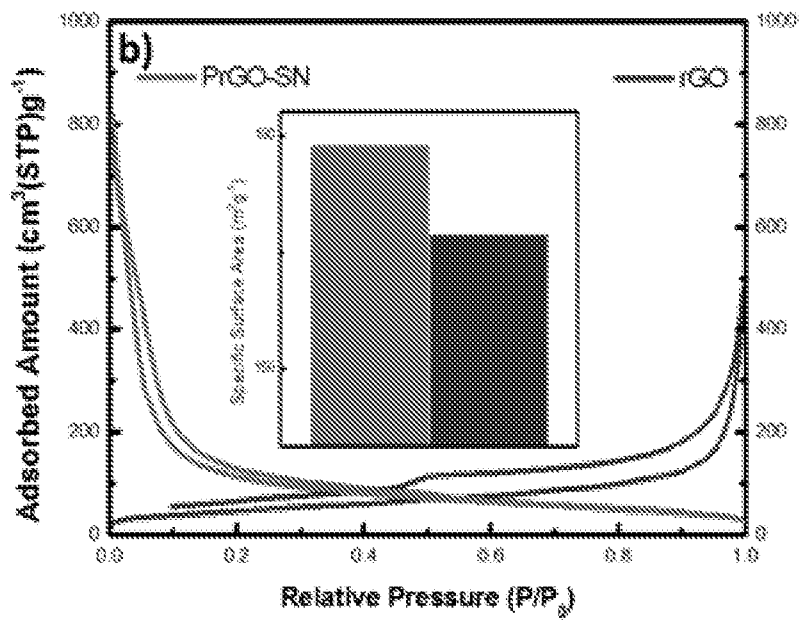


FIG. 6B

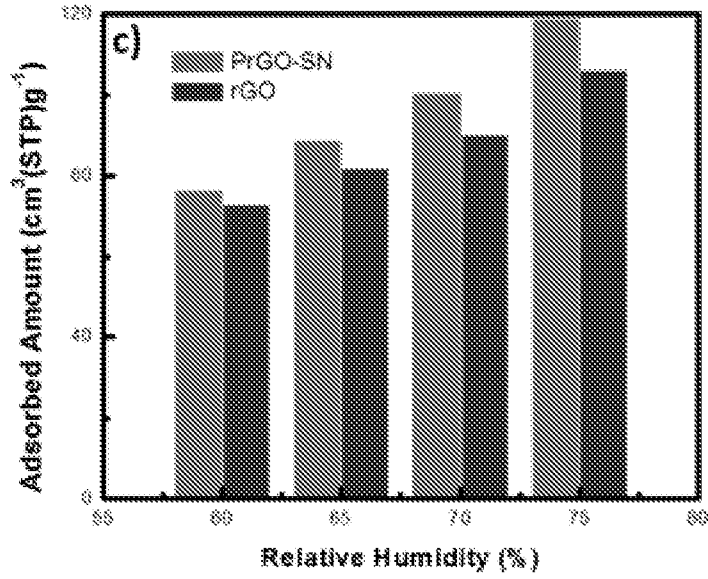


FIG. 6C

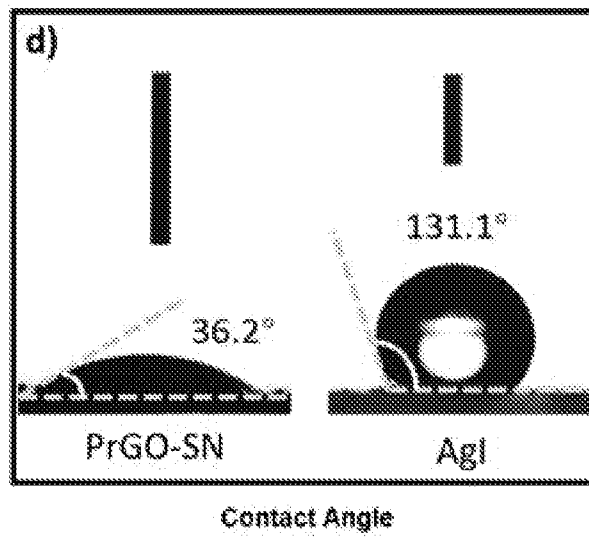


FIG. 6D

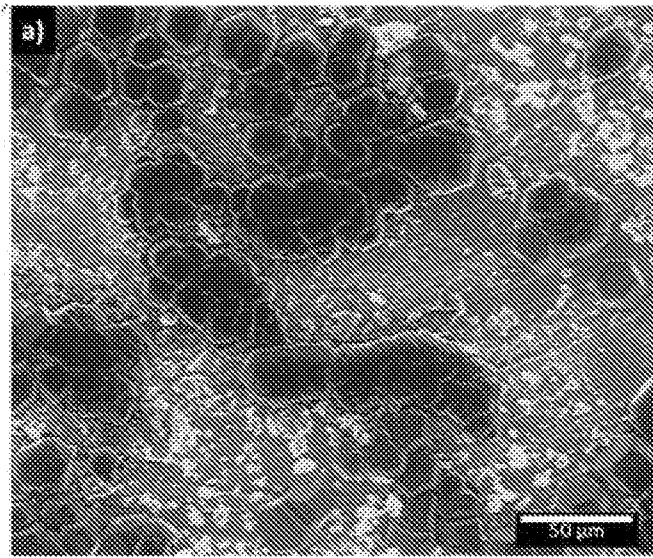


FIG. 7A

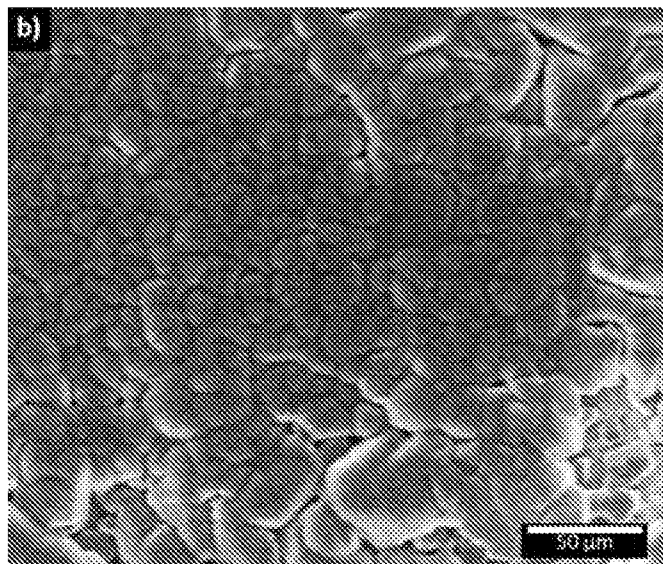


FIG. 7B

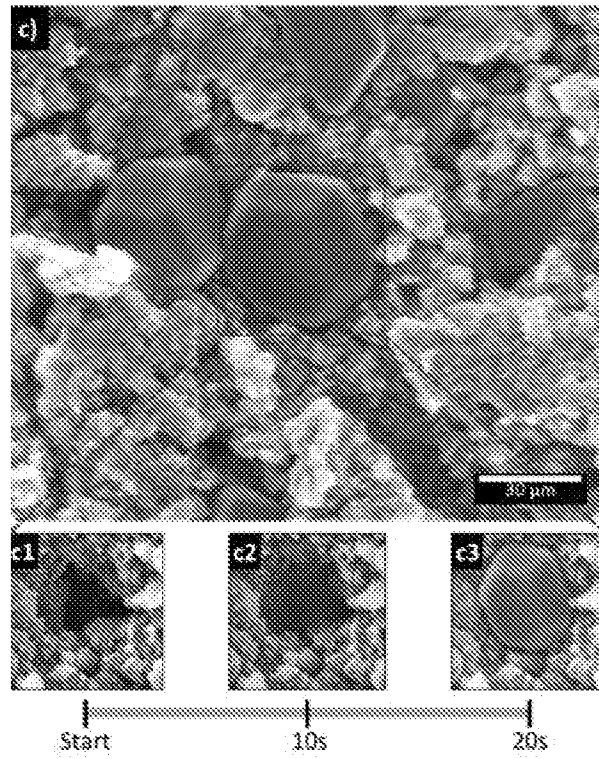


FIG. 7C

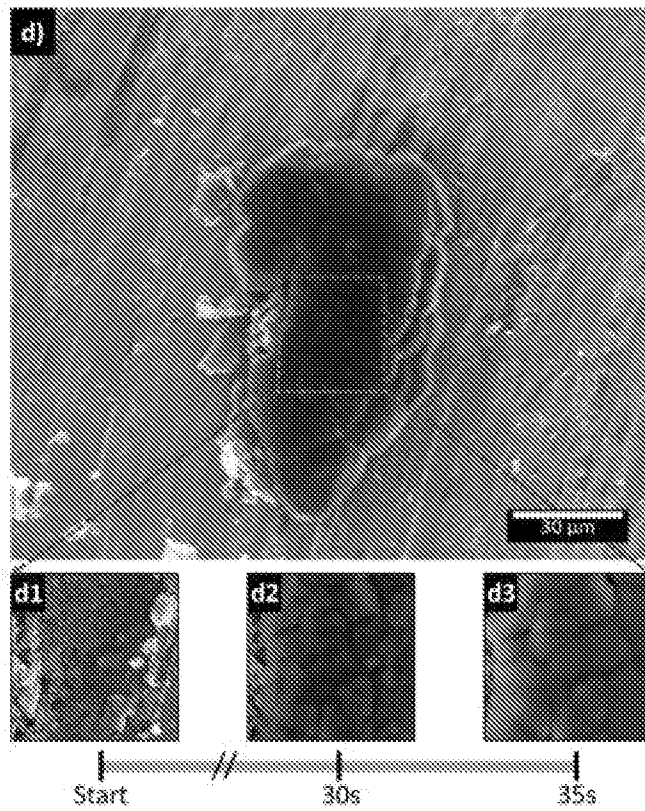


FIG. 7D

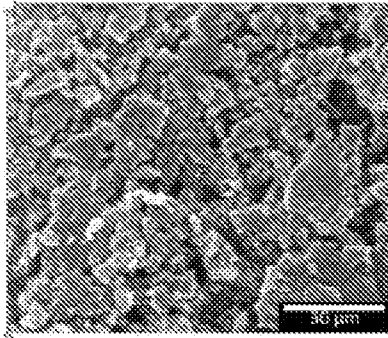


FIG. 8A

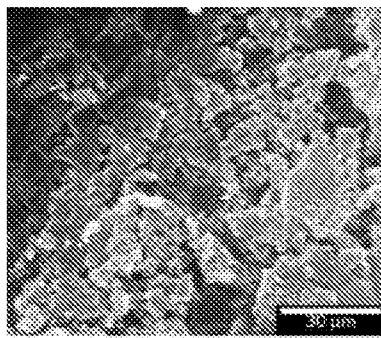


FIG. 8B

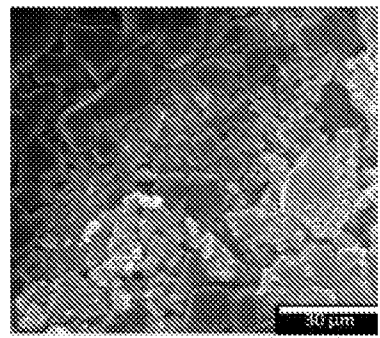


FIG. 8C

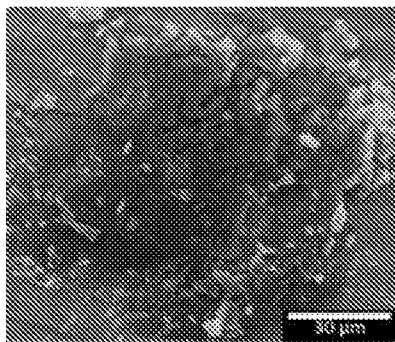


FIG. 8D

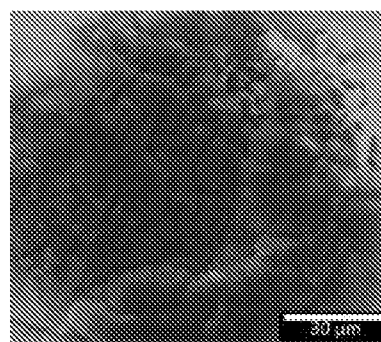


FIG. 8E

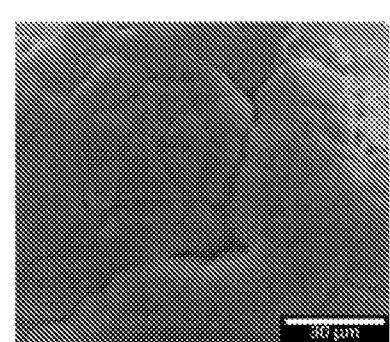


FIG. 8F

INTERNATIONAL SEARCH REPORT

International application No.

PCT / IB 2020/050259

<p>A. CLASSIFICATION OF SUBJECT MATTER IPC: C01B 32/198 (2017.01); C01B 33/00 (2006.01); A01G 15/00 (2006.01); B82Y 30/00 (2011.01) According to International Patent Classification (IPC) or to both national classification and IPC</p>														
<p>B. FIELDS SEARCHED</p> <p>Minimum documentation searched (classification system followed by classification symbols) A01G, B82Y, C01B</p> <p>Documentation searched other than minimum documentation to the extent that such documents are included in the fields searched</p> <p>Electronic data base consulted during the international search (name of data base and, where practicable, search terms used) EPODOC, WPIAP, Fulltext Patentdatabases, XPESP</p>														
<p>C. DOCUMENTS CONSIDERED TO BE RELEVANT</p> <table border="1"> <thead> <tr> <th>Category*</th> <th>Citation of document, with indication, where appropriate, of the relevant passages</th> <th>Relevant to claim No.</th> </tr> </thead> <tbody> <tr> <td>A</td> <td>CN 108862265 A 23 November 2018 (23.11.2018) abstract (UNIV SHENZHEN)</td> <td>1-20</td> </tr> <tr> <td>A</td> <td>WO 2018112575 A1 (UNIVERSIDADE ESTADUAL DE CAMPINAS - UNICAMP, CENTRO NACIONAL DE PESQUISA EM ENERGIA E MATERIAIS - CNPEM) 28 June 2018 (28.06.2018) abstract</td> <td>1-20</td> </tr> <tr> <td>A</td> <td>CN 108246130 A 06 July 2018 (06.07.2018) claims (translated) [online] [retrieved on 20.04.2018]. retrieved from EPOQUE: TXPMTCEU (UNIV JIANGSU)</td> <td>1-20</td> </tr> </tbody> </table>			Category*	Citation of document, with indication, where appropriate, of the relevant passages	Relevant to claim No.	A	CN 108862265 A 23 November 2018 (23.11.2018) abstract (UNIV SHENZHEN)	1-20	A	WO 2018112575 A1 (UNIVERSIDADE ESTADUAL DE CAMPINAS - UNICAMP, CENTRO NACIONAL DE PESQUISA EM ENERGIA E MATERIAIS - CNPEM) 28 June 2018 (28.06.2018) abstract	1-20	A	CN 108246130 A 06 July 2018 (06.07.2018) claims (translated) [online] [retrieved on 20.04.2018]. retrieved from EPOQUE: TXPMTCEU (UNIV JIANGSU)	1-20
Category*	Citation of document, with indication, where appropriate, of the relevant passages	Relevant to claim No.												
A	CN 108862265 A 23 November 2018 (23.11.2018) abstract (UNIV SHENZHEN)	1-20												
A	WO 2018112575 A1 (UNIVERSIDADE ESTADUAL DE CAMPINAS - UNICAMP, CENTRO NACIONAL DE PESQUISA EM ENERGIA E MATERIAIS - CNPEM) 28 June 2018 (28.06.2018) abstract	1-20												
A	CN 108246130 A 06 July 2018 (06.07.2018) claims (translated) [online] [retrieved on 20.04.2018]. retrieved from EPOQUE: TXPMTCEU (UNIV JIANGSU)	1-20												
<input type="checkbox"/> Further documents are listed in the continuation of Box C.		<input checked="" type="checkbox"/> See patent family annex.												
<p>* Special categories of cited documents:</p> <p>“A” document defining the general state of the art which is not considered to be of particular relevance</p> <p>“E” earlier application or patent but published on or after the international filing date</p> <p>“L” document which may throw doubts on priority claim(s) or which is cited to establish the publication date of another citation or other special reason (as specified)</p> <p>“O” document referring to an oral disclosure, use, exhibition or other means</p> <p>“P” document published prior to the international filing date but later than the priority date claimed</p> <p>“T” later document published after the international filing date or priority date and not in conflict with the application but cited to understand the principle or theory underlying the invention</p> <p>“X” document of particular relevance; the claimed invention cannot be considered novel or cannot be considered to involve an inventive step when the document is taken alone</p> <p>“Y” document of particular relevance; the claimed invention cannot be considered to involve an inventive step when the document is combined with one or more other such documents, such combination being obvious to a person skilled in the art</p> <p>“&” document member of the same patent family</p>														
Date of the actual completion of the international search 16 March 2020 (16.03.2020)		Date of mailing of the international search report 30 April 2020 (30.04.2020)												
Name and mailing address of the ISA/AT Austrian Patent Office Dresdner Straße 87, A-1200 Vienna Facsimile No. +43 / 1 / 534 24-535		Authorized officer SLABY S. Telephone No. +43 / 1 / 534 24-348												

INTERNATIONAL SEARCH REPORT
Information on patent family members

International application No.

PCT / IB 2020/050259

Patent document cited in search report			Patent family member(s)			Publication date
CN	A	108862265	CN	A	108862265	2018-11-23
WO	A1	2018112575	WO	A1	2018112575	2018-06-28
			BR	A2	102016030134	2018-08-14
CN	A	108246130	CN	A	108246130	2018-07-06